3D Printing of Ground Tire Rubber Composites

Article *in* International Journal of Precision Engineering and Manufacturing-Green Technology · February 2019

DOI: 10.1007/s40684-019-00023-6

5 authors, including:

Faez Alkadi
University of Akron
6 PUBLICATIONS **83** CITATIONS
SEE PROFILE

Jeongwoo Lee
Hankook Tire - America Technical Center
41 PUBLICATIONS **1,231** CITATIONS
SEE PROFILE

Jun-Seok Yeo
Korea Institute of Industrial Technology
13 PUBLICATIONS **147** CITATIONS
SEE PROFILE

Seok-Ho Hwang
Dankook University
92 PUBLICATIONS **2,847** CITATIONS
SEE PROFILE

International Journal of Precision Engineering and Manufacturing-Green Technology (2019) 6:211–222
https://doi.org/10.1007/s40684-019-00023-6

Online ISSN 2198-0810
Print ISSN 2288-6206

REGULAR PAPER

3D Printing of Ground Tire Rubber Composites

Faez Alkadi[1] · Jeongwoo Lee[1] · Jun-Seok Yeo[2] · Seok-Ho Hwang[2] · Jae-Won Choi[1]

Received: 9 September 2017 / Revised: 20 November 2017 / Accepted: 12 January 2018 / Published online: 11 February 2019

Abstract
Recycled tire rubber is an environmentally and economically beneficial material. Ground tire rubber (GTR) as a filler in a polymer matrix was used as an ink material (composite material) for material extrusion in a 3D printing process. The maximum allowable amount of GTR incorporated into the mixture without significantly altering the rheological behavior of the ink was set. Printability investigations revealed that pressure and speed show linear and power relationships, respectively, to the line width for three different amounts of GTR. Moreover, the post-curing time of 30 min at 115 °C was set as the full-cure condition to achieve polymerization of 80% or more for the 3D printed parts. Unidirectional tensile testing demonstrated that 3D printed specimens exhibit no degradation in tensile strength when compared to molded specimens. Moreover, printability and mechanical properties of functionalized GTR were investigated to determine if this material exhibits enhanced mechanical strength. Unidirectional tensile tests show that the maximum tensile strength for specimens with functionalized GTR was 20% higher than in specimens with non-functionalized GTR. In conclusion, 3D printing of GTR composites shows promise for using recycled GTR to create 3D structures with rubber-like properties.

Keywords 3D printing · Recycled powder · Ground tire rubber · Direct-print · GTR surface modification

List of symbols

GTR	Ground tire rubber
PHR	Part per hundred rubber
DP	Direct-print

✉ Jae-Won Choi
jchoi1@uakron.edu

Faez Alkadi
faa23@zips.uakron.edu

Jeongwoo Lee
jl119@zips.uakron.edu

Jun-Seok Yeo
jsyeo@kitech.re.kr

Seok-Ho Hwang
bach@dankook.ac.kr

[1] Department of Mechanical Engineering, The University of Akron, 244 Sumner St, Akron, OH 44325, USA

[2] Department of Polymer Science and Engineering, Dankook University, Yongin, Gyeonggi 16890, Republic of Korea

1 Introduction

Scrap (waste) tires have become a global environmental issue since they are flammable, non-biodegradable, and contain toxic substances. About 1.5 billion tires are produced every year around the world, and approximately 4 million tons of scrap tires were generated in the US alone in 2015 [1]. Therefore, much research has been conducted to find solutions for the problems related to scrap tires. The research in this area can be classified into two major tracks: (1) how to deal with the scrap tires, and (2) recycling/reusing scrap tires and reclaiming raw materials from them [2–5]. As one method of recycling scrap tires, the production of ground tire rubber (GTR) has been considered due to its positive ecological and economic impacts. The manufacturing process for GTR is environmentally friendly that creates no pollution; it is also economically beneficial, as it eliminates some of the processes needed to reclaim raw rubber. Moreover, the use of GTR as a filler in various raw materials can reduce the cost of manufactured goods [3, 6].

The amount of a filler in a matrix can be directly or inversely proportional to different mechanical properties of composite materials, such as tensile strength, compression strength, and abrasion resistance [7]. Moreover, the interaction of polymer molecules with the surface of fillers can

have a clearly noticeable effect on the mechanical properties of the composite material [8]. Therefore, the composition, properties (e.g. particle size), and processing (e.g. manufacturing method and pre-treatment) of GTR when used as a filler added to a rubber matrix must be considered to obtain the appropriate composite for a given application. An optimal amount of GTR used in composite materials can be determined based on various factors, such as the physical and chemical properties of the GTR, the compatibility between GTR and the matrix materials, and the desired mechanical properties for the resulting product [9–12]. In addition, surface modification and activation of GTR can be used to enhance the mechanical properties of composite materials by increasing the chemical compatibility between GTR and the matrix materials [13–15].

Since 3D printing technology was introduced in the mid-1980s, it has been growing in the automotive, aerospace, and healthcare industries because of the tremendous impact on the manufacturing process, as it allows companies to make customized products without the need for making a mold, especially for items that will not be mass-produced [16–20]. However, one drawback in the 3D printing of polymer materials is that 3D printed pure polymer structures have insufficient strength and functionality. To solve this issue, polymer composites have been considered as printing materials, and the resulting 3D printed polymer composite objects were found to possess more useful structural or functional properties [21]. Furthermore, 3D printing technology has been used as a new recycling approach where printing materials can contain or consist of recyclable materials, which is environmentally and economically beneficial [22, 23]. In this approach, printing materials can take the form of a filament for fused filament fabrication (FFF) or a polymerizable composite for direct-print (DP) 3D printers or other printing processes [21, 23–25]. In FFF 3D printers, recyclable materials can be shredded and mixed in a hot extruder or a recyclebot to produce filaments [23, 25]. For the DP process, ink materials can be in a gelatinous state, which allows a wide variety of composite materials to be used and where it is easier to print with these materials because of their thixotropic behavior [21]. In the DP approach, recycled materials can be shredded or ground for use as an infill material in a matrix [26]. Therefore, print quality can be controlled via printing parameters (tip size, gap distance, printing speed, and/or ink flow rate) to ensure that the material behavior remains within the range for a printable material [27]. The ability to use a wide range of materials makes the DP process superior to other 3D printing processes.

In this study, GTR was used as a filler in a polymer matrix for 3D printable inks/pastes used in the DP process. To print inks, a discharge system with a specific needle tip having a tiny orifice is required [28]. Therefore, to confirm the printability of the inks, different ratios of GTR to polymer matrix were investigated. Moreover, the printing speed and pressure needed for each ratio were studied to maintain the line width for the filament that will result in good printing quality [27]. Two types of GTR (pristine and modified) were used as fillers in polymer composites to compare the effect of the surface modification and the amount of GTR on the resulting 3D printed specimens. In addition, molded specimens with the same type and amount of GTR were fabricated to compare to the 3D printed specimens in terms of mechanical properties.

2 Materials, Methods and Printing Process

2.1 Materials

In this study, TangoPlus FullCure® 930 (FLX930, Stratasys) was used as a polymer matrix. A ground tire rubber (200 mesh) from Edge Rubber (Chambersburg, PA, USA) was used as a filler for 3D printable polymer composites. A fumed silica (M-5 CAB-O-SIL, Cabot Co.) was also added to the 3D printable polymer composites to introduce the thixotropic property. TRIGONOX 125-C750 (AkzoNobel) was used as a thermal initiator for post-curing. Ethyl alcohol (EtOH), 3-(trimethoxysily)propyl methacrylate (TMSPMA), acetic acid, and toluene (ACS reagent, $\geq$ 99.5%) purchased from Sigma-Aldrich were used for modifying the surface of GTR. All chemicals were used as received without further purification.

2.2 Ink Preparation

Pristine or modified GTR was mixed into 15 g of FLX930 polymer matrix (Stratasys Ltd.) at different ratios using a high-speed mixer (SpeedMixer™, FlackTek Inc.) at 2500 rpm for 5 min. To enhance the thixotropic behavior of the printing ink, 1.5 g (10 PHR) of a fumed silica was added to the GTR/FLX930 mixture before it was blended again using the mixer at 2500 rpm for 15 min with mixing beads (the total time was divided into three periods of 5 min each, with 10 min in between to allow the material to cool). The thixotropic behavior is needed to maintain the shape of the printed filament after leaving the tip which helps the printed part to hold itself before curing. When the mixture was cooled to room temperature, 2 wt% of TRIGONOX 125-C750 to the total amount of the mixture was added before mixing at 2500 rpm for 2 min without the mixing beads to prevent a rise in temperature in the ink. Four ink compositions were prepared based on a different amount of GTR (M1, M2, M3, and M4) where GTR amount are 0, 50, 60 and 70 PHR, respectively.

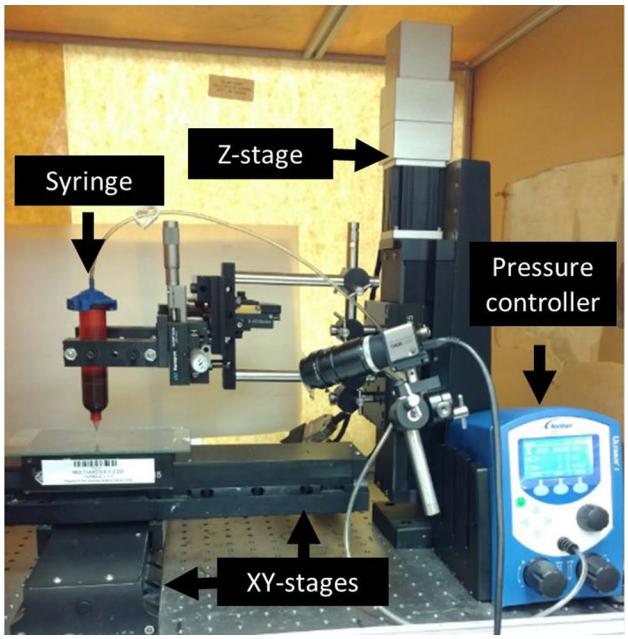

Fig. 1 The DP system used to print the inks

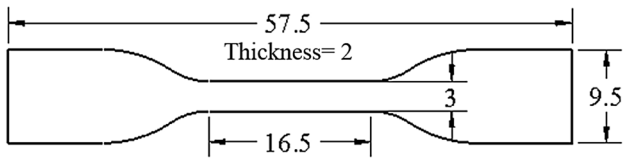

Fig. 2 Dimensions of a dogbone tensile test specimen (all dimensions are given in mm)

2.3 Printing System

A customized DP system was used to print the prepared inks. The system consists of a pressure controller (Ultimus™ I, Nordson EFD) and a motorized XYZ linear stage (PRO115, Aerotech), where a syringe was installed on the Z stage (Fig. 1). The pressure controller and the XYZ linear stage were synchronized using G-code instructions in Aerotech control interfaces and LabVIEW.

2.4 3D Printing Process

A 3D model of a dogbone specimen for tensile testing was designed using a 3D modeling program (SolidWorks®). The specimens were designed according to the dimensions of a Type IV tensile bar in ASTM D638-14 (after scaling it to half the size) as shown in Fig. 2. The model was then exported as an STL (stereolithography) file to an open-source hosting program (Repetier-Host, Hot-World GmbH), which has a built-in slicing tool (Slic3r) that converts the STL file into layers and generates motion instructions (G-code) for 3D printing. The layer thickness was adjusted during the slicing process based on the tip size used (335 µm ID). Infill percentage and fill angle for the 3D printed specimens were 100% and 0°, respectively. The material was loaded into a syringe immediately after preparation to prevent any changes in the material properties that might occur due to changes in temperature and/or oxygen content over time. Next, the material in the syringe was re-mixed using the high-speed mixer at 2500 rpm for 1 min to remove any air bubbles in the mixture. Finally, the syringe was connected to the pressure controller and placed on the XYZ stage to begin 3D printing. Various discharging pressures and speeds were investigated to obtain the optimal printing parameters for different printing inks while maintaining the requisite tip size (335 µm) and gap distance (300 µm).

2.5 Conversion of FLX930 in M2 Composition

The polymerization and crosslinking of the FLX930/silica mixtures was achieved using TRIGONOX 125-C750 as a liquid thermal initiator. The reaction was carried out in a hot oven at 115 °C for various time durations (5, 10, 20, 30, 40, and 50 min) to confirm the appropriate reaction time. After polymerization/crosslinking, five specimens (~ 30 mg each) were cut from the M2 rubber/silica composite dogbone sample. This selection was made because M2 has the highest FLX930 to GTR ratio compared to M3 and M4, and the exact weight (W_0) was measured on a precision balance. Each specimen was soaked in a vial containing 30 ml of toluene and kept at room temperature for 24 h to remove unreacted species. The specimens were then soaked in ethyl alcohol for 3 h to remove the toluene, and they were dried in an oven at 100 °C for 24 h to remove any remaining ethyl alcohol. Finally, the weight of the dried specimens (W_1) was measured. Percentage conversion for the specimens was calculated gravimetrically by using formula (1):

$$\text{Conversion}(\%) = \frac{W_1}{W_0} \times 100 \quad (1)$$

2.6 Surface Modification of GTR

The surface modification of GTR was performed as one step of the hydrolysis–condensation reaction shown in Fig. 3 [29]. A total of 10 g of TMSPMA as a silane coupling agent was added to distilled water (300 ml), and the solution was adjusted to a pH of 2 by adding acetic acid. Next, a pristine GTR (10 g) was added to the solution (after being washed with ethyl alcohol to remove unwanted chemicals) and stirred for 24 h at 65 °C. The product was filtered and washed with the EtOH/H_2O mixture (3/7; v/v) and then dried in a vacuum dry oven at 80 °C.

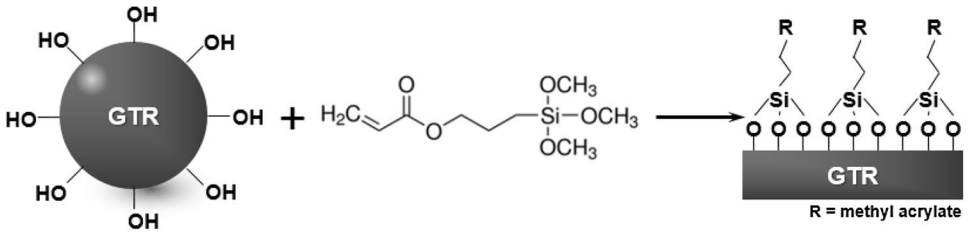

Fig. 3 Schematic illustration of the hydrolysis–condensation reaction between TMSPMA and hydroxyl groups on the GTR surface

2.7 Characterization

The surface modification of GTR was characterized by Fourier-transform infrared spectroscopy (FTIR) using a Nocolet S10 (Thermo Scientific). The morphological study of the GTR/rubber composites was confirmed by field emission scanning electron microscopy (FE-SEM) using a JSM-7100F (JEOL USA) at 10 kV. The width of the printed lines was measured using a stereomicroscope (SteREO Discovery.V.12, Carl Zeiss Micro Imaging). To investigate the effect of the manufacturing process (3D printed or molded) and amount of GTR (50 PHR or 70 PHR) on the mechanical properties of three composite materials, unidirectional tensile testing was conducted using an Instron® 5567 tensile tester (Instron Corp.) with a ± 1-kN static load cell at a speed of 5 mm/s.

3 Results and Discussion

3.1 Printability

The modified composite material is 3D printable, which is an important property for achieving the goal of comparing the 3D printed specimens to the molded specimens. Experiments on printability were conducted to establish a relationship between the printing parameters and the desired line width. To confirm the printability of GTR/FLX930 composite inks, the DP process was conducted under various printing pressures and speeds. For both pressure and speed experiments, the measurement of the width of a given line was taken as the mean value of ten different points on the same line. To maintain consistency in the measurement locations, a marker pen was used to draw five parallel lines in the *X*-direction on the substrate before the start of the printing process. These five lines were positioned so that they would intersect with the lines to be printed in the *Y*-direction, forming an intersection point (marked with rectangles in Fig. 5a) that would be measured to obtain the linewidth. In this way, we can ensure that the distance between all 10 points (where a filament is printed in the positive and negative *Y*-directions, forming five intersection points in each direction) are the same for every single line (for both pressure and speed) to prevent any inconsistency in measurement.

Figure 4 shows the marking line and the filaments printed at different speeds. Figure 4a shows the marking process where five parallel lines were drawn in the *X*-direction. These five lines are equidistant, as explained previously. Figure 4b–d show filaments printed in the *Y*-direction at speeds of 5 mm/s, 15 mm/s and 35 mm/s, respectively. The results of this experiment for composition M2 at different pressure and speed values are shown in Fig. 5.

Figure 5a shows six sets of lines of GTR/FLX930 composite (M2) printed with pressures from 7 to 12 psi in 1-psi increments at a speed of 20 mm/s. The GTR/FLX930 composite ink (M2) starts discharging from the nozzle at 7 psi, and the width of the printed line increases with the pressure. At 12 psi, the line width reaches about 200% of the inner diameter of the nozzle. This indicates that the printing pressure is directly related to the line width of the printed material [30]. In addition, the effect of the printing speed on the width of lines can be seen in Fig. 5b, where the pressure was observed to be different for each material composition (M2, M3 and M4) based on data from the pressure effect experiment. The M2 material composition was used as an example to show the effect of speed on the width of the line. Nine lines were printed with different speeds (5–45 mm/s, in increments of 5 mm/s) at a pressure of 9.5 psi (Fig. 5b). The speed range was related to the line continuity, where the test starts at 5 mm/s for all material compositions (M2, M3 and M4), and stops when the line begins to disconnect.

Figure 6 shows the relationship between printing parameters (pressure and speed) and line width, where other parameters (tip size and gap height) were fixed for M2, M3 and M4. As shown in Fig. 6a, each different material composition ratio (M2, M3 and M4) requires a different amount of pressure to achieve the same line width. This pressure ratio difference is based on the rheological property of the material, which is directly related to the amount of GTR. The result shows that the higher the GTR content, the higher the pressure required. Figure 6b shows the relationship between print speed and line width. The same three material compositions (M2, M3 and M4) were tested, and a specific pressure was set for each material composition based on the results shown in Fig. 6a, where a 500 μm line width was taken as a reference line width for all material compositions (M2, M3 and M4). In the speed tests, the same pressure (9.5 psi) was applied on all material composition.

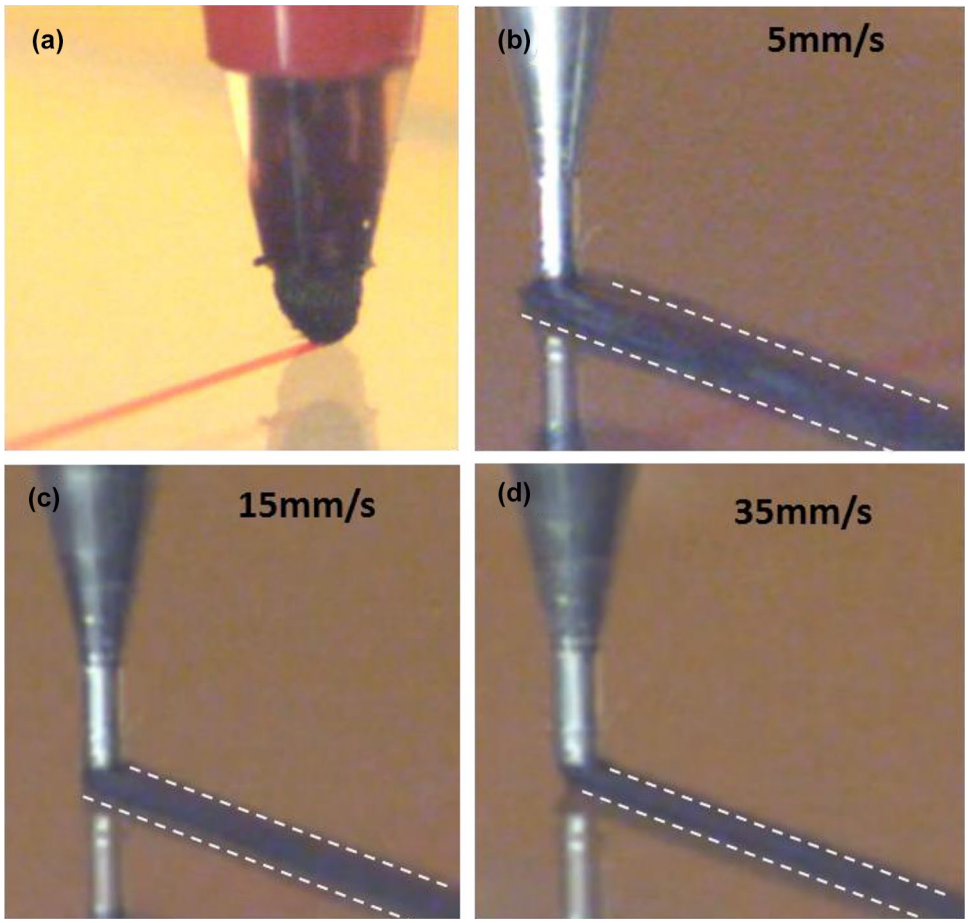

Fig. 4 Substrate marking experiment: **a** Line made in the *X*-direction using the marker pen, **b**–**d** Filaments with different printing speeds

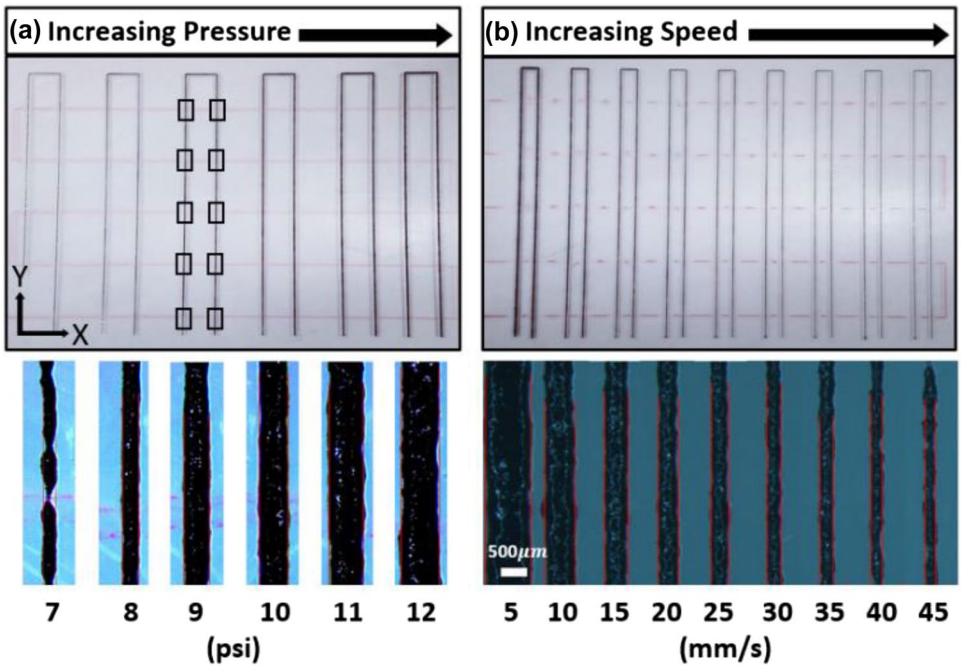

Fig. 5 Microscope images of printed lines **a** under different printing pressure from 7 to 12 psi at speed 20 mm/s and **b** at different printing speed from 5 to 45 mm/s under 9.5 psi pressure

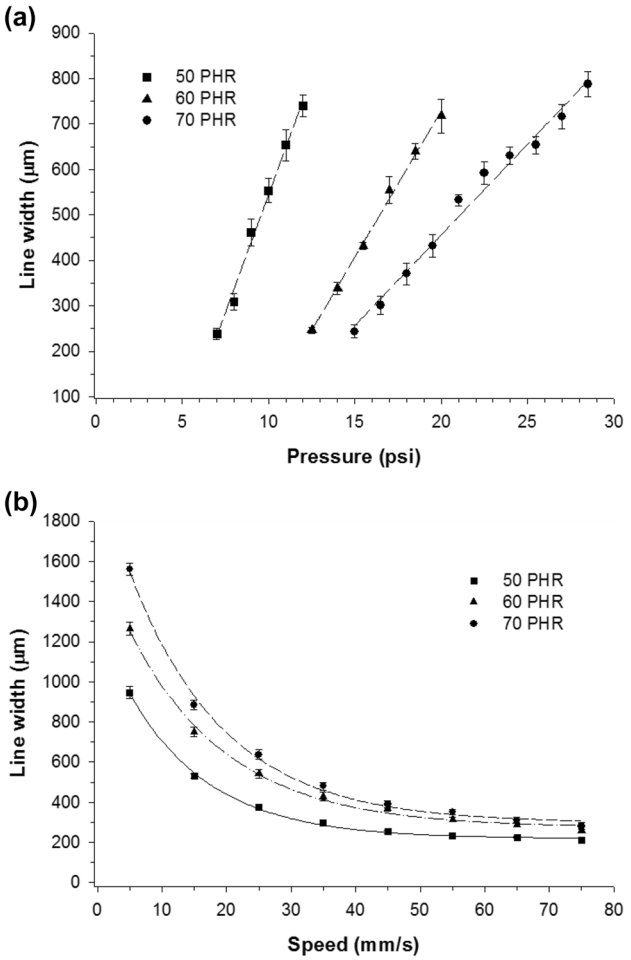

Fig. 6 Correlation between the width of printed lines and the print parameters **a** pressure and **b** speed for GTR/FLX930 composite materials with different amounts of GTR (M2, M3 and M4) at a fixed tip size (335 μm) and gap distance (268 μm)

Based on the pressure and speed tests, the pressures for printing M2, M3 and M4 were set at 9.5 psi, 16.5 psi and 21 psi, respectively. The results in Fig. 6 show that printed line widths can be controlled by several factors such as the printing parameters or material properties. In particular, the material behavior plays a key role in maintaining the filament shape when the printing parameters such as pressure and speed are set [27, 31].

3.2 Conversion of FLX930 in M2 Composition

Because monomer conversion is an important factor in improving the mechanical properties of polymer materials, the reaction time and temperature need to be investigated as the main factors driving the conversion process [32]. In this study, the reaction temperature was maintained at 115 °C while various reaction times were investigated to confirm the proper reaction time. Figure 7 shows the effect of different

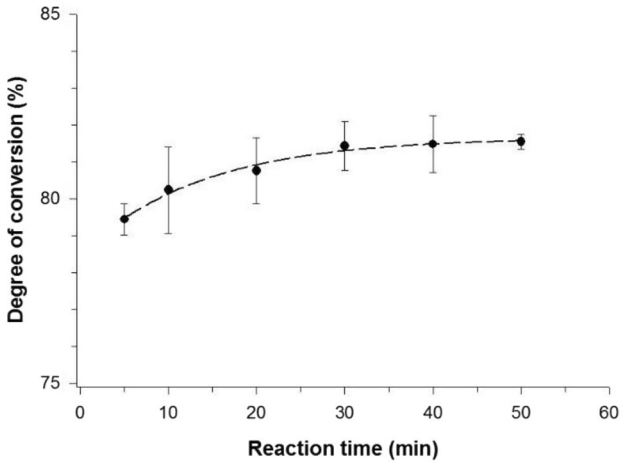

Fig. 7 Degree of conversion of FLX930 in M2 composition for different reaction time at 115 °C

reaction times on the conversion of material M1, which contains 2 wt % of a thermal initiator. The percentage conversion is in the range of 79.5–81.5% and converges on 81.5% after 30 min. Thus, a time of 30 min was determined to be the proper reaction time in this study.

3.3 3D Printed Structures

3D structures were fabricated to show the capability of the prepared material in the developed system (Fig. 1) by controlling the printing parameters. These printing parameters were set for each material composition based on the printability experiment described in Sect. 3.1. Figure 8 presents the process for manufacturing a tire tread using the prepared composite M2. In the first step of the manufacturing process (Fig. 8a), the CAD model of the tire tread is designed using SolidWorks®. Figure 8b shows the second step, where the tool path is generated using a built-in slicing program (Slic3r) in the host program (Repetier-Host). After the tool path is obtained, the next step is the actual 3D printing process (Fig. 8c). The last step is thermal curing, where the final tread is produced after baking 30 min at 115 °C (Fig. 8d). The high quality of the printed product demonstrates the high capability of the composed material to be used as an ink material for the DP 3D printing process.

To investigate the mechanical properties of the printed composite material, dogbone test specimens were fabricated using material composites M2 and M4 (Fig. 9a). Infill settings for these 3D printed specimens were set so the printed specimens would be comparable to molded specimens (as will be discussed in Sect. 3.4). Figure 9b shows the smooth discharge of the filament from the nozzle tip during fabrication of specimens based on suitable printing parameters (pressure, speed and gap distance).

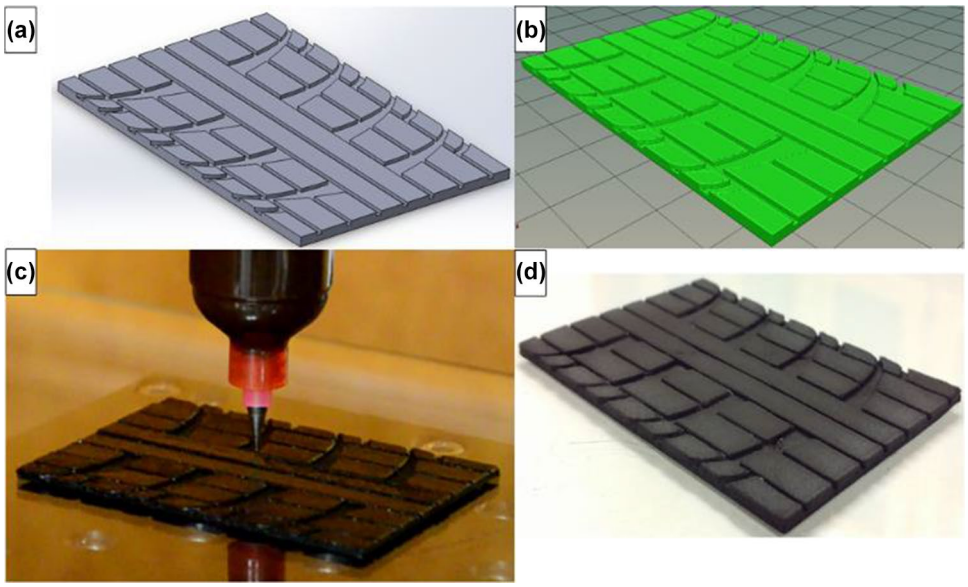

Fig. 8 3D-printed tire tread of GTR composite material: **a** CAD model of the tire tread, **b** Generating a tool path with a slicing program, **c** Actual 3D printing of the tire tread, **d** Final product

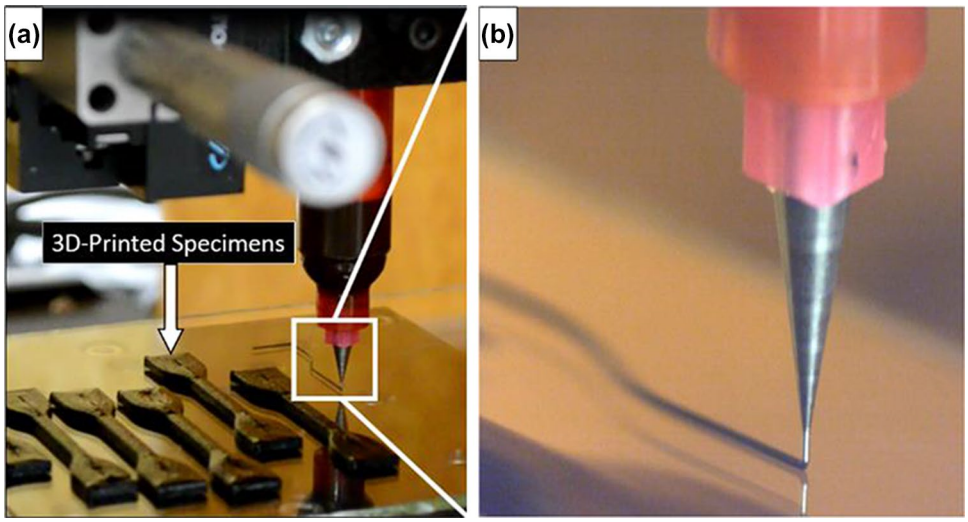

Fig. 9 Fig. Printing process: **a** fabricated dogbone specimens, **b** Magnified photograph of the printing process

3.4 Tensile Tests: Effect of Manufacturing Method

Unidirectional tensile tests were conducted to investigate the effect of the manufacturing method (3D printed and molded specimens) and the amount of GTR (by comparing specimens prepared using M2 and M4) on the composite material (ink material). In terms of the manufacturing process, the tests show that there is almost no difference in tensile strength when comparing the 3D printed specimens to the molded ones for both M2 and M4 material compositions (Fig. 10). This result is attributed to the fill density (100%) of the 3D printed specimens, leading to interfilament melt fusion, which closes the gap between the printed lines when they touch one another and results in a solid cross section for the printed specimens [33]. Fill angle can play a significant role in the maximum stress for 3D printed specimens; [34] thus, all 3D printed specimens were printed at a fill angle of 0°. These printing conditions helped the 3D printed specimens maintain nearly the same tensile strength as the molded specimens (Fig. 10). Since there is almost no difference in tensile strength for the 3D printed parts, this implies that it is possible to customize parts without causing a degradation in the mechanical properties.

The ratio of a filler material to a matrix material can also affect the mechanical properties of a composite material. Figure 10 shows a lower tensile strength obtained for specimens prepared using M2 compared to specimens with M4 for both 3D printed and molded specimens. This degradation in the tensile strength for specimens prepared using M4 is attributed to the aggregation of GTR particles in the composite material, since aggregation is known to increase with GTR content. Therefore, the aggregations act as mechanical failure concentration points (failure initiation sites) [35, 36]. It is obvious that different amounts of GTR content

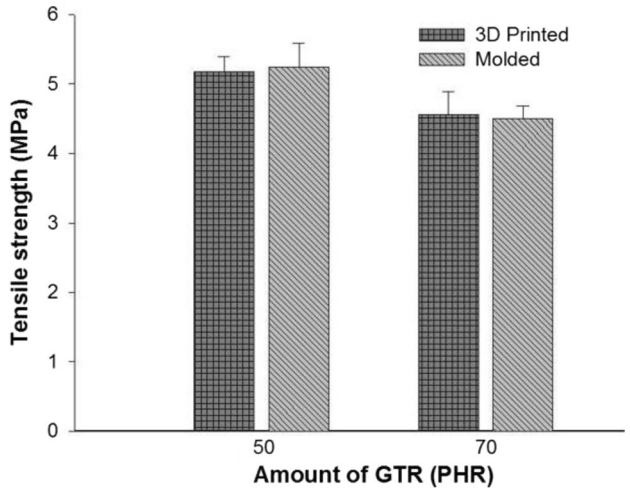

Fig. 10 Ultimate tensile strength of 3D-printed and molded specimens with different material compositions: M2 and M4 (50 and 70 PHR, respectively)

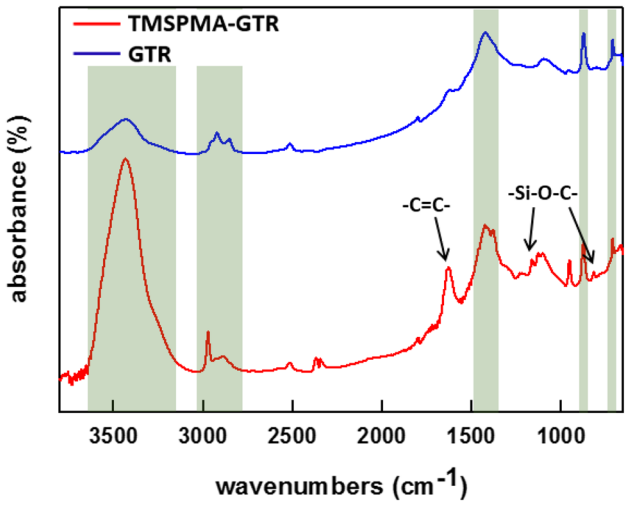

Fig. 11 FTIR spectra of pristine GTR (blue line) and modified GTR (red line)

will result in products with different tensile strengths. This relation between the GTR content and tensile strength could be linear or non-linear, directly or inversely proportional. Further investigation on the GTR content will be carried out in the future work.

3.5 Surface Modification of GTR

Chemical modification of a GTR surface as a filler should improve the adhesion strength between the filler and polymer matrix in the polymeric composites. In this study, GTR modified by the silane coupling agent (TMSPMA-GTR) was obtained by using a one-step hydrolysis–condensation reaction. In the first step, which is well known from the previous literature [29], the hydrolyzable alkoxy group in the presence of moisture leads to the formation of silanols. In the next step, the silanol reacts with a hydroxyl group on the GTR surface to form stable siloxane covalent bonds.

FTIR analysis was carried out to ascertain the chemical linkage between the silane coupling agents and GTR surface. Figure 11 shows the normalized FTIR spectra of the pristine GTR and the TMSPMA-GTR. The pristine GTR in Fig. 11 (indicated by the blue line) shows some characteristic peaks: hydrogen bonded –OH stretching (around 3800–2995 cm^{-1}), –CH stretching (around 2900 cm^{-1}), $–CH_2$ bending (around 1430 cm^{-1}), –CH bending or $-CH_2$ stretching (around 900 cm^{-1}, which indicates an amorphous structure), and –OH out-of-plane bending (around 687 cm^{-1}).

In addition, the normalized FTIR spectra of the TMSPMA-GTR (indicated by the red line in Fig. 11) shows positive evidence of the chemical linkage between the GTR surface and TMSPMA, where new peaks appear around 1330 cm^{-1} and 780 cm^{-1} that originate from the hydrolysis–condensation reaction resultant peak (–Si–O–C) on the TMSPMA-GTR. The appearance of a peak related to C=C bonding (which appears around 1600 cm^{-1}) shows that a large amount of vinyl moieties were anchored on the GTR surface.

To investigate the interaction between the GTR particles and the rubber matrices, the fractured surface of the composites was observed using FE-SEM after conducting tensile tests on the GTR/rubber composites. A larger number of holes arise from the loss of pristine GTR particles (Fig. 12a) compared to the number arising from the loss of particles from the modified GTR/rubber composite (Fig. 12c). The morphology of the pristine GTR/rubber composite (Fig. 12b) shows a visible lack of adhesion between the GTR particle and the rubber matrix compared to the modified GTR/rubber composite (Fig. 12d). The terminal vinyl group (–C=C–) on the surface of the modified GTR can react with the rubber matrix during polymerization/curing, resulting in increasing the interaction between the GTR particles and rubber matrix as shown in Fig. 13.

3.6 Tensile Tests: Effect of GTR Content

In polymer composites, filler particles are employed to enhance the modulus and reinforce softer polymer matrices since the rigid filler particles generally have a much higher stiffness compared to polymer matrices. And the high surface area of fillers provides many contact sites between the fillers and polymer matrices. Therefore, the improved properties in polymer composites come from the strong interfacial interactions between fillers and polymer matrices. Figure 14 shows the difference in tensile strength between specimens with different GTR contents (M1, M2 and M4).

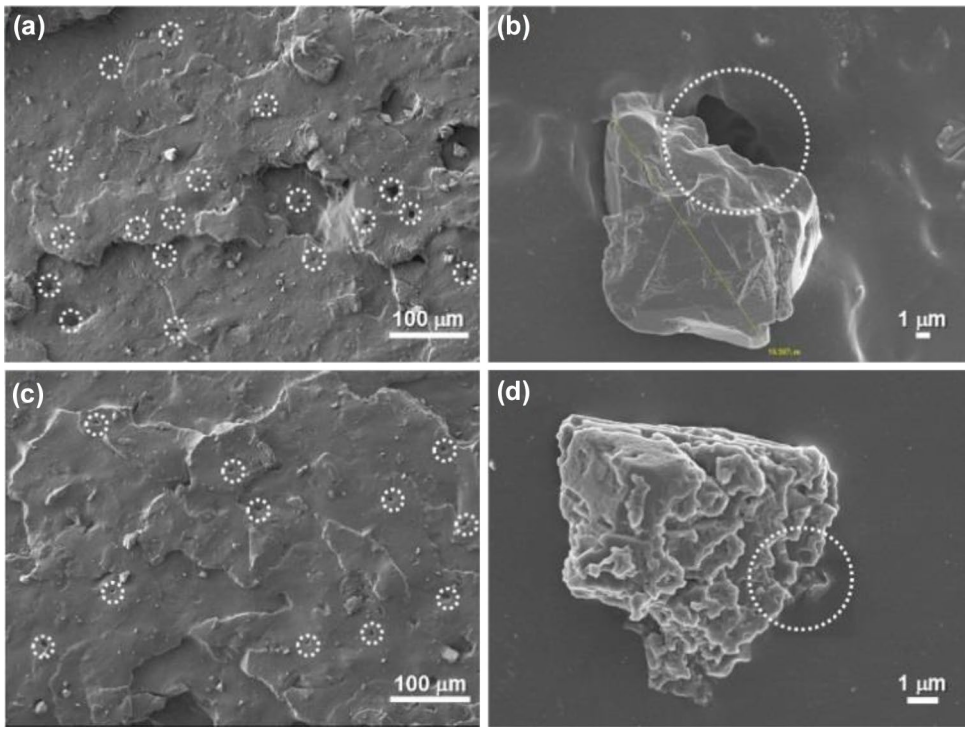

Fig. 12 SEM photographs of GTR/rubber composites: **a**, **b** pristine GTRs and **c**, **d** modified GTRs

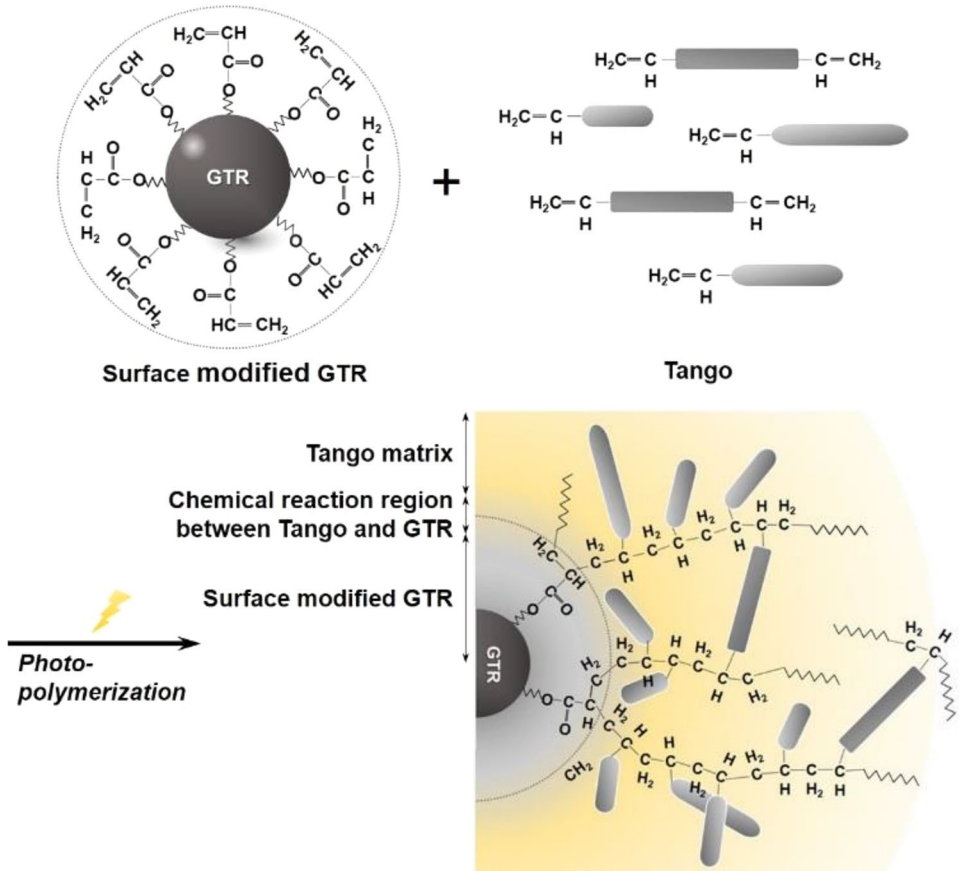

Fig. 13 Schematic illustration showing the reaction of the terminal vinyl on the surface of the modified GTR with the rubber matrix during polymerization

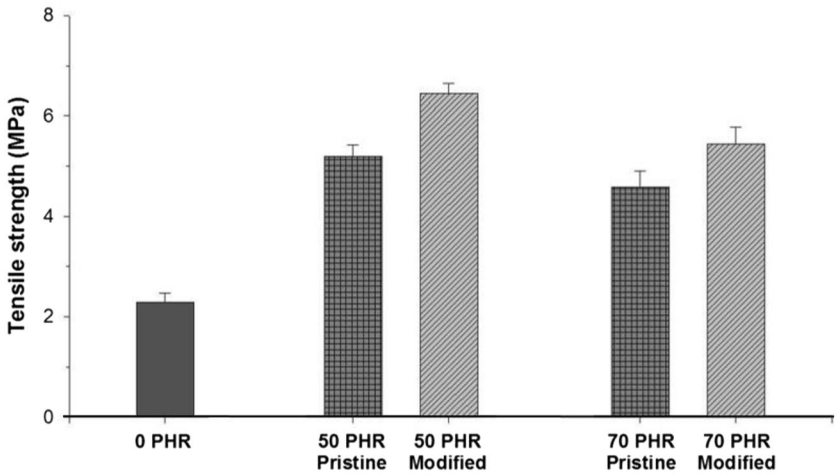

Fig. 14 Ultimate tensile strength of the pristine GTR/FLX930 and modified GTR/FLX930 composites with different material compositions: M1, M2 and M4 (0, 50, and 70 PHR, respectively)

As can be seen in this figure, specimens with no GTR content (M1) exhibited a very low tensile strength as compared to other specimens. This difference in tensile strength is attributed to the stiffness enhancement obtained by adding GTR particles to the polymer matrix [35, 36].

Compatibility between the filler material and the matrix material can affect the mechanical properties of the final composite material [35]. The effect of the surface modification of the GTR particles on the dispersion quality has improved the tensile strength of the printed specimens [37, 38]. Figure 14 shows the effect of the GTR type (pristine versus modified) for material compositions M2 and M4 (50 PHR and 70 PHR, respectively) on the tensile strength of the 3D printed specimens. As can be noticed from this figure, the modified GTR has a positive influence on the tensile strength, where it shows more than 20% improvement due to the better dispersion of the GTR in the rubber matrix following modification. The increase in tensile strength is attributed to the good compatibility between the GTR and the polymer matrix. This good compatibility makes the bonds between the GTR and the polymer matrix stronger than the tendency for agglomeration. As agglomeration decreases, the interface zone between the GTR and the polymer matrix increases; this leads to a higher interfacial interaction, resulting in more bonding between the GTR particles and polymer matrix, which results in a composite with higher tensile strength [35, 39].

4 Conclusions

This study demonstrates the capability for reusing recycled GTR for 3D printing. The GTR can be used as a filler in the polymer matrix to form a composite material that can be used as a printing ink for the DP process. Printability experiments have shown that pressure and speed have a direct influence on the print quality. Also, the experiment conducted to investigate the conversion quality of FLX930 in the M2 material has shown that 30 min is the minimum time required for the developed composite material to be fully cured at a temperature of 115 °C). After fixing the printing parameters and curing conditions, 3D structures were fabricated to demonstrate the ability of the developed material to be used as an ink material for the DP process. The results show that 3D printed specimens have nearly the same tensile strength as molded specimens. Moreover, surface modification of GTR has been shown to improve the tensile strength of the 3D printed specimens. This work will help to reduce the environmental impact by re-using recycled GTR from scrap tires as a filler material in polymer matrix, and also reduce the printed part price through using less amount of polymer matrix. Further investigations on improving mechanical properties using different coupling agents and increasing the amount of GTR will be accomplished in future.

Acknowledgements The first author has been financially supported by Jazan University and Saudi Arabian Cultural mission (SACM) during the completion of this work. The authors also would like to thank Mr. Md Omar Faruk Emon at The University of Akron, USA, for providing the tire tread design that was used for the 3D printred tire tread in this study.

References

1. Czajczynska, D., Krzyzynska, R., Jouhara, H., & Spencer, N. (2017). Use of pyrolytic gas from waste tire as a fuel: A review. *Energy, 134,* 1121–1131. **(In Press)**.
2. Adhikari, B., De, D., & Maiti, S. (2000). Reclamation and recycling of waste rubber. *Progress in Polymer Science, 25*(7), 909–948.
3. Fang, Y., Zhan, M. S., & Wang, Y. (2001). The status of recycling of waste rubber. *Materials and Design, 22*(2), 123–127.
4. De, D., Das, A., Dey, B., Debnath, S. C., & Roy, B. C. (2006). Reclaiming of ground rubber tire (GRT) by a novel reclaiming agent. *European Polymer Journal, 42*(4), 917–927.

5. Wu, B., & Zhou, M. H. (2009). Recycling of waste tyre rubber into oil absorbent. *Waste Management, 29*(1), 355–359.
6. Burford, R., & Pittolo, M. (1982). Characterization and performance of powdered rubber. *Rubber Chemistry and Technology, 55*(5), 1233–1249.
7. Rattanasom, N., Saowapark, T., & Deeprasertkul, C. (2007). Reinforcement of natural rubber with silica/carbon black hybrid filler. *Polymer Testing, 26*(3), 369–377.
8. Stockelhuber, K. W., Svistkov, A. S., Pelevin, A. G., & Heinrich, G. (2011). Impact of filler surface modification on large scale mechanics of styrene butadiene/silica rubber composites. *Macromolecules, 44*(11), 4366–4381.
9. Rattanasom, N., Poonsuk, A., & Makmoon, T. (2005). Effect of curing system on the mechanical properties and heat aging resistance of natural rubber/tire tread reclaimed rubber blends. *Polymer Testing, 24*(6), 728–732.
10. Segre, N., & Joekes, I. (2000). Use of tire rubber particles as addition to cement paste. *Cement and Concrete Research, 30*(9), 1421–1425.
11. Rattanasom, N., Prasertsri, S., & Ruangritnumchai, T. (2009). Comparison of the mechanical properties at similar hardness level of natural rubber filled with various reinforcing-fillers. *Polymer Testing, 28*(1), 8–12.
12. Sonnier, R., Leroy, E., Clerc, L., Bergeret, A., Lopez-Cuesta, J. M., Bretelle, A. S., et al. (2008). Compatibilizing thermoplastic/ground tyre rubber powder blends: Efficiency and limits. *Polymer Testing, 27*(7), 901–907.
13. Shanmugharaj, A. M., Kim, J. K., & Ryu, S. H. (2005). UV surface modification of waste tire powder: Characterization and its influence on the properties of polypropylene/waste powder composites. *Polymer Testing, 24*(6), 739–745.
14. Song, X. F., Wang, Z. B., & Wang, B. X. (2016). Mechanical properties, morphology, and Mullins effect of thermoplastic elastomers based on polypropylene and waste ethylene–propylene–diene terpolymer powder compatibilized by styrene–butadiene–styrene block copolymer. *Journal of Thermoplastic Composite Materials, 29*(3), 410–424.
15. Hernandez, E. H., Gamez, J. F. H., Cepeda, L. F., Munoz, E. J. C., Corral, F. S., Rosales, S. G. S., et al. (2017). Sulfuric acid treatment of ground tire rubber and its effect on the mechanical and thermal properties of polypropylene composites. *Journal of Applied Polymer Science, 134,* 21.
16. Vehseto, M., & Seitz, H. (2014). A new micro-stereolithography-system based on diode laser curing (DLC). *International Journal of Precision Engineering and Manufacturing, 15*(10), 2161–2166.
17. Weller, C., Kleer, R., & Piller, F. T. (2015). Economic implications of 3D printing: Market structure models in light of additive manufacturing revisited. *International Journal of Production Economics, 164,* 43–56.
18. Prasad, D. (2015). Additive manufacturing—a brief foray into the advancements in manufacturing technologies. *International Journal of Advance Industrial Engineering, 3*(3), 115–119.
19. Ho, C. M. B., Ng, S. H., & Yoon, Y. J. (2015). A review on 3D printed bioimplants. *International Journal of Precision Engineering and Manufacturing, 16*(5), 1035–1046.
20. Lee, J., Kim, H. C., Choi, J. W., & Lee, I. H. (2017). A review on 3D printed smart devices for 4D printing. *International Journal of Precision Engineering and Manufacturing-Green Technology, 4*(3), 373–383.
21. Wang, X., Jiang, M., Zhou, Z., Gou, J., & Hui, D. (2017). 3D printing of polymer matrix composites: A review and prospective. *Composites: Part B, 110,* 442–458.
22. Chong, S., Chiu, H. L., Liao, Y. C., Hung, S. T., & Pan, G. T. (2015). Cradle to Cradle (R) Design for 3D printing. *Pres15, 45,* 1669–1674.
23. Braanker, G., Duwel, J., Flohil, J., & Tokaya, G. (2010). *Developing a plastics recycling add-on for the RepRap 3D printer*. Delft: Delft University of Technology, Prototyping Lab.
24. Kreiger, M. A., Mulder, M. L., Glover, A. G., & Pearce, J. M. (2014). Life cycle analysis of distributed recycling of post-consumer high density polyethylene for 3-D printing filament. *Journal of Cleaner Production, 70,* 90–96.
25. Feeley, S. R., Wijnen, B., & Pearce, J. M. (2014). Evaluation of potential fair trade standards for an ethical 3-D printing filament. *Journal of Sustainable Development, 7*(5), 1.
26. Truby, R. L., & Lewis, J. A. (2016). Printing soft matter in three dimensions. *Nature, 540*(7633), 371–378.
27. Vatani, M., Engeberg, E. D., & Choi, J. W. (2013). Force and slip detection with direct-write compliant tactile sensors using multi-walled carbon nanotube/polymer composites. *Sensors and Actuators a-Physical, 195,* 90–97.
28. Hon, K. K. B., Li, L., & Hutchings, I. M. (2008). Direct writing technology-Advances and developments. *CIRP Annals-Manufacturing Technology, 57*(2), 601–620.
29. Agrawal, R., Saxena, N. S., Sharma, K. B., Thomas, S., & Sreekala, M. S. (2000). Activation energy and crystallization kinetics of untreated and treated oil palm fibre reinforced phenol formaldehyde composites. *Materials Science and Engineering a-Structural Materials Properties Microstructure and Processing, 277*(1–2), 77–82.
30. Li, J. P., de Wijn, J. R., Van Blitterswijk, C. A., & de Groot, K. (2006). Porous Ti6Al4V scaffold directly fabricating by rapid prototyping: Preparation and in vitro experiment. *Biomaterials, 27*(8), 1223–1235.
31. Chen, C.-P., Li, H.-X., & Ding, H. (2007). Modeling and control of time-pressure dispensing for semiconductor manufacturing. *International Journal of Automation and Computing, 4*(4), 422–427.
32. Vallittu, P. K., Ruyter, I. E., & Buykuilmaz, S. (1998). Effect of polymerization temperature and time on the residual monomer content of denture base polymers. *European Journal of Oral Sciences, 106*(1), 588–593.
33. Miller, J. S., Stevens, K. R., Yang, M. T., Baker, B. M., Nguyen, D. H. T., Cohen, D. M., et al. (2012). Rapid casting of patterned vascular networks for perfusable engineered three-dimensional tissues. *Nature Materials, 11*(9), 768–774.
34. Le, X., Akouri, R., Latassa, A., Passemato, B., Wales, R. (2016). In *Mechanical Property Testing and Analysis of 3D Printing Objects*, ASME 2016 International Mechanical Engineering Congress and Exposition, American Society of Mechanical Engineers. pp. V002T02A059–V002T02A059.
35. Mirjalili, F., Chuah, L., & Salahi, E. (2014). Mechanical and morphological properties of polypropylene/nano alpha-Al2O3 composites. *Scientific World Journal*. https://doi.org/10.1155/2014/718765.
36. Huang, L., Zhan, R. B., & Lu, Y. F. (2006). Mechanical properties and crystallization behavior of polypropylene/nano-SiO_2 composites. *Journal of Reinforced Plastics and Composites, 25*(9), 1001–1012.
37. Kango, S., Kalia, S., Celli, A., Njuguna, J., Habibi, Y., & Kumar, R. (2013). Surface modification of inorganic nanoparticles for development of organic–inorganic nanocomposites—A review. *Progress in Polymer Science, 38*(8), 1232–1261.
38. Zhang, X. X., Zhu, X. Q., Liang, M., & Lu, C. H. (2009). Improvement of the properties of ground tire rubber (GTR)-filled nitrile rubber vulcanizates through plasma surface modification of GTR powder. *Journal of Applied Polymer Science, 114*(2), 1118–1125.
39. Akil, H. M., Lily, N., Abd Razak, J., Ong, H., & Ahmad, Z. A. (2006). Effect of various coupling agents on properties of alumina-filled PP composites. *Journal of Reinforced Plastics and Composites, 25*(7), 745–759.

Faez Alkadi Ph.D. candidate in the Department of Mechanical Engineering at The University of Akron. His research interests include conformal 3D printing and process planning.

Jeongwoo Lee Postdoc researcher in the Department of Mechanical Engineering at The University of Akron. His research focuses on preparation of pre-polymer composites for the Direct-print photopolymerization.

Jun-Seok Yeo Postdoc researcher in the Human Convergence Technology Group at Korea Institute of Industrial Technology(KITECH). His research interest is surface treatment technology for composites and textronics.

Seok-Ho Hwang Associate Professor in the department of Polymer Engineering at Dankook University. His research interests are design and synthesis of functional polymers, organic materials for semi-conductor processes, organic electronic materials and eco-friendly polymers.

Jae-Won Choi Associate Professor in the Department of Mechanical Engineering at The University of Akron. His research interests are 3D printing and additive manufacturing, 3D printed smart structures including sensors, actuators and electronics, 3D printed rubbers including insoles and tires, biofabrication and low-cost binder-coated metal/ceramic for 3D printing.